

Convective heat transport in stratified atmospheres at low and high Mach number

Evan H. Anders and Benjamin P. Brown

*Department of Astrophysical & Planetary Sciences, University of Colorado – Boulder and
Laboratory for Atmospheric and Space Physics, Boulder, CO*

Here we study stratified convection in the context of polytropically stratified atmospheres. We hold the density stratification and Prandtl number (Pr) constant while studying the dependence of the Nusselt number (Nu), which quantifies the efficiency of convective heat transport, on variations of the Mach number (Ma) and the Rayleigh number (Ra). In the low Ra regime, high and low Ma flows have very different scalings of Nu with Ra . In the high Ra regime, high and low Ma flows have nearly the same scaling of Nu with Ra , with power laws near (enter here), reminiscent of the $\text{Nu} \propto \text{Ra}^{2/7}$ seen in Rayleigh-Bénard convection.

INTRODUCTION

Convection is essential to heat transport in the cores of high mass stars, the envelopes of low mass stars, and the atmospheres of terrestrial and jovian planets. In such systems, convection occurs in the presence of the atmospheric stratification, which can be small but extends up to 14 density scale heights in the Sun’s convective envelope. A basic understanding of the properties of compressible convection in stratified media is important to understanding systems in astrophysics and planetary sciences. Numerical constraints typically have restricted studies of stratified convection to moderately high Mach numbers, appropriate to regions near the Sun’s surface. As such, we know little about the fundamental properties of low-Mach number stratified convection, which occurs in the deep solar interior.

Some of the earliest numerical experiments on stratified convection were performed in two [1–4] and three [5, 6] dimensions and revealed a number of basic properties in the moderate-to-high Mach number regime. Unlike the widely-studied Rayleigh-Bénard problem, in which upflows and downflows are symmetrical, highly stratified convection exhibits high-velocity, narrow downflow lanes and slow, broad upflow lanes. As velocities approach the speed of sound, shocks begin to form near the downflow lanes at the top of the atmosphere and propagate toward the upflows. In Rayleigh-Bénard convection, the temperature gradient and by proxy the radiative flux approach zero in the convecting region. In stratified convection, the *entropy* gradient is flattened by convection, but this does not necessitate the disappearance of the radiative flux due to contributions of thermodynamic variables other than temperature to the entropy.

In Rayleigh-Bénard convection, there exist two primary control parameters: the Rayleigh number (Ra), the ratio of buoyant driving to diffusive damping, and the Prandtl number (Pr), the ratio of viscous to thermal diffusivity. Along with the aspect ratio of the physical domain, these two numbers entirely control the dynamics of the convection. In stratified atmospheres, in addition to specifying the equation of state and funda-

mental properties of the gas, the two control parameters of Rayleigh-Bénard convection are joined by the degree of stratification across the domain and the characteristic Mach number (Ma) of the convective flows. Polytropically stratified atmospheres, such as those used in early studies, are an ideal extension of Rayleigh-Bénard convection into the stratified realm as the two additional control parameters are directly linked to basic properties of the atmosphere. The density stratification is set by the number of density scale heights the atmosphere spans (n_ρ), and the Mach number is controlled by the superadiabatic excess (ϵ), which is the deviation of the polytropic index from that of an adiabatic polytropic index [1].

In this letter, we study the effects of variations of ϵ and Ra on the heat transport of convection in polytropically stratified atmospheres, characterized by the Nusselt number (Nu). We hold n_ρ and Pr constant across all simulations and examine moderate (4) and large (8) aspect ratios. In section II, we describe the construction of atmospheres, our equations, and our method for numerical time evolution. We describe our findings in section III and discuss implications in section IV.

EXPERIMENT

In order to compare our results with previous studies and in an effort to examine a simplest case, we study a fluid composed of monatomic ideal gas particles, with an adiabatic index of $\gamma = 5/3$ and whose equation of state is $P = R^* \rho T$. The initial stratification is polytropic, such that the gravitational acceleration and conductive heat flux are invariant throughout the depth of the atmosphere. In order to satisfy the latter assumption, the thermal conductivity, κ and temperature gradient ∇T_0 are often taken as constants, such that $\mathbf{F}_{\text{cond},0} = -\kappa \nabla T_0 = \text{constant}$. Under these assumptions, solving the equation of hydrostatic equilibrium produces an atmosphere defined by

$$\begin{aligned}\rho_0(z) &= \rho_{00}(z_0 - z)^m \\ T_0(z) &= T_{00}(z_0 - z),\end{aligned}\tag{1}$$

where z increases upwards within the bounds $z = \{0, L_z\}$. We specify the number of density scale heights the atmosphere spans, n_ρ , to determine L_z . Throughout this letter, we set $n_\rho = 3$ such that the density at the bottom of the atmosphere is larger than at the top by a factor of 20. Thermodynamic variables are nondimensionalized at the top of the atmosphere as $P_0(L_z) = \rho_0(L_z) = T_0(L_z) = 1$, requiring $z_0 \equiv L_z + 1$ and $R^* = T_{00} = \rho_{00} = 1$. The polytropic index is set by the adiabatic index and the superadiabatic excess, ϵ , such that $m = m_{ad} - \epsilon$ where $m_{ad} \equiv (\gamma - 1)^{-1}$ is the adiabatic polytropic index. The subsequent entropy gradient at the top of the atmosphere is $\nabla S(L_z) = -\epsilon$, the negative of the superadiabatic excess. The characteristic timescale of such an atmosphere is related to the characteristic atmospheric buoyancy time, $t_b = \sqrt{L_z/g\epsilon}$. We will utilize buoyancy time units throughout this letter.

Atmospheric diffusivities are set by the Rayleigh number and the Prandtl number. We define the non-dimensional Rayleigh number as

$$\text{Ra} = \frac{gL_z^3(\Delta S_0/c_P)}{\nu\chi}, \quad (2)$$

where ΔS_0 is the entropy difference between the top and bottom of the atmosphere, ν is the kinematic viscosity (viscous diffusivity), and χ is the thermal diffusivity. The relationship between the thermal and viscous diffusivities is set by the Prandtl number, $\text{Pr} = \nu/\chi$. We relate the dynamic viscosity, μ , and the thermal conductivity, κ , to their corresponding diffusivities such that $\nu \equiv \mu/\rho$ and $\chi \equiv \kappa/\rho$. As a result, $\text{Ra} \propto (\nu\chi)^{-1} \propto \rho^2$, such that for our atmospheres with $n_\rho = 3$, the Rayleigh number increases by a factor of 400 from the top of the domain to the bottom of the domain. Such a formulation leaves Pr constant throughout the depth of the atmosphere, and in this letter we impose $\text{Pr} = 1$.

At the constant values of n_ρ and Pr used, the primary control parameters of convection are ϵ and Ra . We decompose our atmosphere into the background polytrope ($\ln \rho_0, T_0$) and the fluctuations about that background ($\mathbf{u}, \ln \rho_1, T_1$). The scaling of the entropy gradient with ϵ is reflected in the evolved values of these fluctuations, which follow the scaling of $\text{Ma}^{1/2} \propto T_1/T_0 \propto \rho_1/\rho_0 \propto \epsilon$, and which scale as roughly $\text{Ra}^{0.3}$, as in Fig. 1.

We evolve the Fully Compressible Navier-Stokes equations, which take the form:

$$\frac{D \ln \rho}{Dt} + \nabla \cdot (\mathbf{u}) = 0 \quad (3)$$

$$\rho \frac{D\mathbf{u}}{Dt} = -\nabla P + \rho \mathbf{g} - \nabla \cdot \bar{\bar{\Pi}} \quad (4)$$

$$\begin{aligned} \rho c_V \left(\frac{DT}{Dt} + (\gamma - 1)T \nabla \cdot (\mathbf{u}) \right) + \nabla \cdot (-\kappa \nabla T) = \\ - (\bar{\bar{\Pi}} \cdot \nabla) \cdot \mathbf{u} \end{aligned} \quad (5)$$

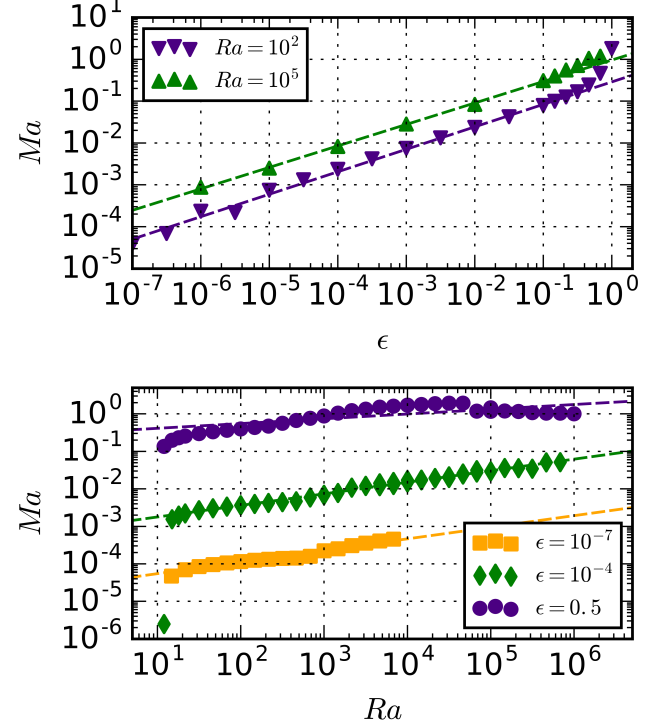


FIG. 1. (a) Characteristic horizontally averaged maximum Mach numbers which have been time averaged over $100t_b$ starting roughly $100t_b$ after the start of simulations. At low ϵ , Ma shows power laws of $\text{Ma} \propto \epsilon^{0.5048}, \epsilon^{0.5129}$ at $\text{Ra} = 10^2$ and 10^5 , respectively (need err bars). When $\epsilon \rightarrow m_{ad}$, large deviations from this power law are seen and the system quickly approaches $\text{Ma} \approx 1$. Ma shows weak scaling with ϵ , and does not exceed $\text{Ma} \approx 1$

where $D/Dt \equiv \partial_t + \mathbf{u} \cdot \nabla$ and the viscous stress tensor is defined as

$$\Pi_{ij} \equiv -\mu \left(\frac{\partial u_i}{\partial x_j} + \frac{\partial u_j}{\partial x_i} - \frac{2}{3} \delta_{ij} \nabla \cdot (\mathbf{u}) \right). \quad (6)$$

In such stratified systems, the total convective flux can be defined as

$$\mathbf{F}_{\text{conv}} \equiv \mathbf{F}_{\text{enth}} + \mathbf{F}_{\text{KE}} + \mathbf{F}_{\text{PE}} + \mathbf{F}_{\text{visc}}, \quad (7)$$

where $\mathbf{F}_{\text{enth}} \equiv \rho \mathbf{u} (c_V T + P/\rho)$ is the enthalpy flux, $\mathbf{F}_{\text{KE}} \equiv \rho |\mathbf{u}|^2 \mathbf{u}$ is the kinetic energy flux, $\mathbf{F}_{\text{PE}} \equiv \rho \mathbf{u} \phi$ is the potential energy flux (with $\phi \equiv -gz$), and $\mathbf{F}_{\text{visc}} \equiv \mathbf{u} \cdot \bar{\bar{\Pi}}$ is the viscous flux. Taking an inner product of Eq. 4 with \mathbf{u} and adding it to Eq. 5, the full energy equation in conservation form is retrieved,

$$\frac{\partial}{\partial t} \left(\rho \left[\frac{|\mathbf{u}|^2}{2} + c_V T + \phi \right] \right) + \nabla \cdot (\mathbf{F}_{\text{conv}} + \mathbf{F}_{\text{rad}}) = 0 \quad (8)$$

where $\mathbf{F}_{\text{rad}} = -\kappa \nabla T$. An understanding of the flux terms is essential to characterizing the convective heat transport in our systems.

The atmosphere is bounded above and below by impenetrable, stress free, fixed temperature boundary conditions such that

$$w = \partial_z u = T_1 = 0 \quad (9)$$

at the boundaries.

We utilize the novel Dedalus pseudospectral framework (cite website?) to time-evolve Eqs. 3-5 using an implicit-explicit third-order four-step Runge-Kutta timestepping scheme [7]. Variables are time-evolved on a dealiased Chebyshev (vertical) and Fourier (horizontal, periodic) domain in which the physical grid dimensions are 3/2 the size of the coefficient grid. Our physical grid sizes range from 96x384 grid points at the lowest values of Ra to 1152x4608 grid points at $\text{Ra} \geq 10^7$. By using IMEX timestepping, we are able to study flows at moderate ($Ma \approx 1$) and very low ($Ma \approx 10^{-4}$) Mach number (Fig. 1b).

RESULTS

The efficiency of convection is quantified by the Nusselt number. While the Nusselt number is well-defined in Rayleigh-Bénard convection as the amount of total flux divided by the steady-state background conductive flux [8, 9], a well-defined Nusselt number is more elusive in stratified convection. A traditional definition of the Nusselt number in stratified convection is [1, 3]

$$N \equiv \frac{F_{\text{conv}, z} + F_{\text{rad}, z} - F_A}{F_{\text{ref}} - F_A}, \quad (10)$$

where $F_{\text{conv}, z}$ and $F_{\text{rad}, z}$ are the z-components of \mathbf{F}_{conv} and \mathbf{F}_{rad} , respectively. F_A is the adiabatic conductive flux, defined as $F_A = -\kappa \partial_z T_{\text{ad}}$. For an atmosphere in hydrostatic equilibrium, such as a polytrope, $\partial_z T_{\text{ad}} \equiv -g/c_P$, and thus $F_A = \kappa g/c_P$. $F_{\text{ref}} = \Delta T/L_z$ is the conductive flux of a linear profile connecting the upper and lower plates, where $\Delta T = T_u - T_\ell$.

We contend that this is the general form of the Nusselt number. To illustrate this, we consider a few limiting cases. Convection works to suppress entropy stratification and create isentropic atmospheres. Under the Boussinesq approximation where density variations are ignored, entropy stratification is directly proportional to temperature stratification, such that $\nabla S \rightarrow 0$ only when $\nabla T \rightarrow 0$. Thus, for Rayleigh-Bénard convection, $\nabla T_{\text{ad}} \equiv 0$ and the familiar form of N is retrieved. In the case of stratified convection, as $\epsilon \rightarrow m_{ad} + 1$, $\nabla P \propto g \rightarrow 0$ and the resulting $\nabla T_{\text{ad}} \rightarrow 0$. In such a case, $F_A \rightarrow 0$ and the familiar definition of the Rayleigh-Bénard nusselt number is appropriate to use, which explains why convection carries all of the atmospheric flux in such a case [10]. As $\epsilon \rightarrow 0$, $\nabla T_{\text{ad}} \rightarrow \nabla T_0$, the atmospheric initial temperature profile. This causes increasingly smaller

velocity, temperature, and pressure perturbations (e.g. Fig. 1), but due to the removal of the background radiative flux from the numerator and denominator in Eq. 10, increasingly smaller perturbations have just as large of an effect on the nusselt number.

We solved initial value problems which start in hydrostatic and thermal equilibrium and experienced infinitesimal kicks compared to ϵ in T_1 . Solutions were time-evolved until a long-time average of N showed little dependence on height. At high values of ϵ , shock systems form in the upper atmosphere near downflow lanes (see e.g. Fig. 2a) and propagate towards upflow lanes. Such systems were reported in both two [4] and three [11] dimensional polytropic simulations previously. Low mach number flows, such as those in an $\epsilon = 10^{-4}$ atmosphere (e.g. Fig. 2b) have similar bulk thermodynamic structure but lack the complicating dynamics of shock heating. As Ra is increased to very large values (e.g. Fig. 2c), thermodynamic structures no longer span the vertical extent of the domain but instead break up into small packets which traverse through the domain many times before diffusing. The complicated nature of high Ra dynamics, especially in the low Ma regime where shocks are absent, has barred us from sufficiently converging any solutions in the regime of $\text{Ra} > 10^7$.

Despite different thermodynamic structures, the properly normalized *sum* of the fluxes for a given Ra is similar. See, for example, Fig. 3 to see time-averaged horizontal profiles of the vertical system fluxes. At high ϵ and Ra, \mathbf{F}_{enth} and \mathbf{F}_{KE} exhibit two local maxima over the depth of the domain, whereas at low ϵ and low Ma, there is only one local maximum near the bottom of the domain. Viscous fluxes become important near the bottom boundary layer, and radiative flux is nearly zero everywhere in the domain except for near the boundaries where the fixed-temperature boundary conditions create large deviations in ∇T away from ∇T_{ad} .

At low Rayleigh number, diffusivities are high and the flows are very laminar. Such flows often achieve a steady state and have a well-defined Nusselt number which is independent of time. However, as the Rayleigh number increases, the flows become increasingly time-dependent. Even steady structures such as solid “rolls” like those pictured in Fig. 2 have highly time-dependent Nusselt numbers. This is, in part, due to the fact that cold downdrafts floating to the bottom of the domain can be entrained by upflows, or warm risen parcels can be entrained in the intense cold downdrafts. Such events reverse the preferred direction of flux in the system, and even let the Nusselt number become negative for short periods of time. As a result, it is necessary to take a long time average of the fluxes before calculating the Nusselt number at higher Rayleigh number. (IS THIS USEFUL?)

The evolution of the Nusselt number as the Rayleigh number is increased is shown for both high and low ϵ in Fig. 4. Below convective onset, the Nusselt number is

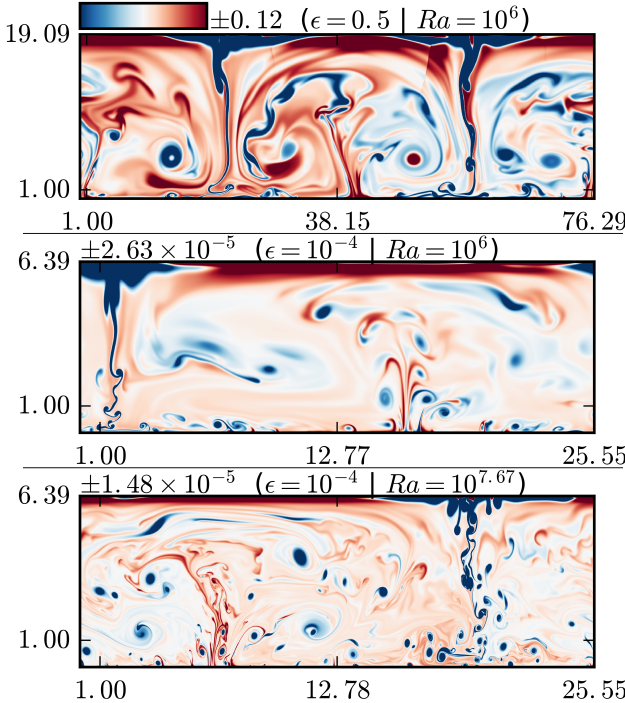


FIG. 2. Characteristic entropy. The time- and horizontally-averaged profile is removed in all cases. At high ϵ (a), shock systems form near the upper downflow lanes and propel shock-heated material deep within the atmosphere at sufficiently high Ra . At low ϵ but at the same Ra (b), shock systems are absent, but otherwise the dynamics are similar. As Ra is increased (c), downflow lanes no longer span the entirety of the domain and individual cold, small blobs are responsible for carrying the flux downward.

perfectly one. Just above onset, there is a brief range of highly inflated scaling between N and Ra .

DISCUSSION

acknowledgements

This work was supported by the CU/NSO Hale Graduate Fellowship and Juri's allocation and Ben's allocation. We thank Axel Brandenburg, Mark Rast, and Jeff Oishi for many useful discussions.

- [1] E. Graham, Journal of Fluid Mechanics **70**, 689 (1975).
- [2] K. L. Chan, S. Sofia, and C. L. Wolff, Astrophys. J. **263**, 935 (1982).
- [3] N. E. Hurlbert, J. Toomre, and J. M. Massaguer, Astrophys. J. **282**, 557 (1984).
- [4] F. Cattaneo, N. E. Hurlbert, and J. Toomre, ApJL **349**, L63 (1990).

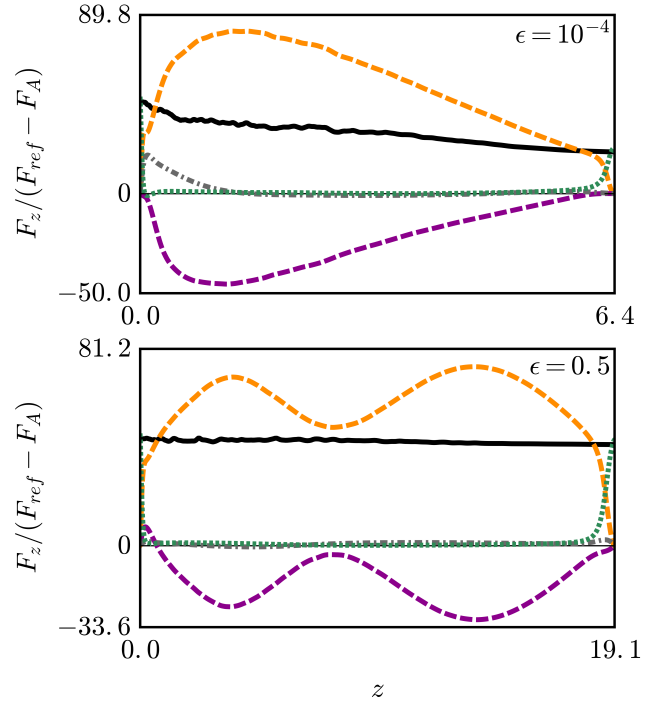


FIG. 3. Flux profiles for low (top) and high (bottom) Mach number flows.

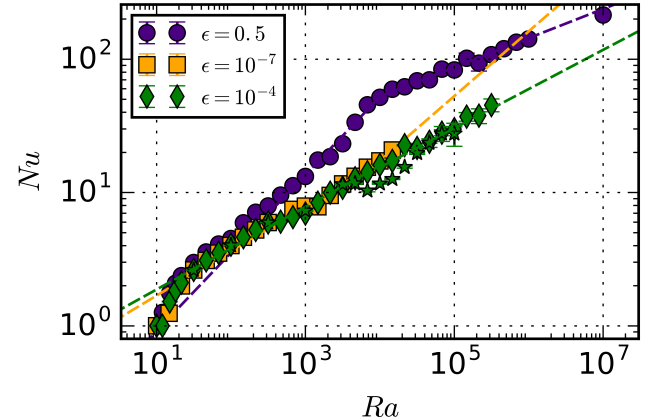


FIG. 4. Variation of the Nusselt number as a function of the Rayleigh number is shown.

- [5] F. Cattaneo, N. H. Brummell, J. Toomre, A. Malagoli, and N. E. Hurlbert, Astrophys. J. **370**, 282 (1991).
- [6] N. H. Brummell, N. E. Hurlbert, and J. Toomre, Astrophys. J. **473**, 494 (1996).
- [7] U. M. Ascher, S. J. Ruuth, and R. J. Spiteri, Applied Numerical Mathematics **25**, 151 (1997).
- [8] H. Johnston and C. R. Doering, Physical Review Letters **102**, 064501 (2009), 0811.0401.
- [9] J. Otero, R. W. Wittenberg, R. A. Worthing, and C. R. Doering, Journal of Fluid Mechanics **473**, 191 (2002).

- [10] A. Brandenburg, K. L. Chan, Å. Nordlund, and R. F. Stein, *Astronomische Nachrichten* **326**, 681 (2005), astro-ph/0508404.
- [11] A. Malagoli, F. Cattaneo, and N. H. Brummell, *ApJL* **361**, L33 (1990).